Asian Journal of Chemical Sciences

9(2): 1-13, 2021; Article no.AJOCS.64778
ISSN: 2456-7795

Crystal Growth and Structure Determination of a Newly Synthesised Chalcone Derivative with Hirshfeld Surface Analysis and Energy Frame Work: (2e,4e)-5-(4-(Dimethylamino)Phenyl)-1-(Naphthalen-2-Yl)Penta-2,4-Dien-1-One

M. Krishna Priya[1], D. Reuben Jonathan[2], K. Biruntha[3], D. Angeline Shirmila[1], K. Laavanya[1], J. Hemalatha[1] and G. Usha[1*]

[1]PG and Research Department of Physics, Queen Mary's College (A), Affiliated to the University of Madras, Chennai-04, Tamil Nadu, India.
[2]Department of Chemistry, Madras Christian College, Affiliated to the University of Madras, Chennai-59, Tamilnadu, India.
[3]Department of Physics, Bharathi Women's College, Affiliated to the University of Madras, Chennai-108, Tamil Nadu, India.

Authors' contributions

This work was carried out in collaboration among all authors. Author MKP helped in conceptualization, software analysis, data Validation, wrote original draft of the manuscript. Author DRJ performed Methodology. Author KB performed data validation. Authors DAS and KL wrote and edited the manuscript. Author JH performed data validation. Author GU performed validation of data, data curation and supervised the study. All authors read and approved the final manuscript.

Article Information

DOI: 10.9734/AJOCS/2021/v9i219065
Editor(s):
(1) Dr. Sung Cheal Moon, Korea Institute of Materials Science (KIMS), Republic of Korea.
Reviewers:
(1) Hasaneen Kudhair Abdul labass, Alkut University College, Iraq.
(2) Chandra Shekhara Shetty, St Aloysius College Mangalore, India.
Complete Peer review History: http://www.sdiarticle4.com/review-history/64778

Original Research Article

Received 05 November 2020
Accepted 10 January 2021
Published 01 February 2021

ABSTRACT

A new chalcone derivative (*2E, 4E*)-5-(4-(dimethylamino) phenyl)-1-(naphthalen-2-yl) penta-2,4-dien-1-one (DPNP) has been synthesized using Claisen-Schmidt condensation reaction using the slow evaporation method at ambient temperature. The 3D crystal structure was solved using the

**Corresponding author: E-mail: guqmc@yhoo.com;*

single-crystal X-ray diffraction method (XRD). XRD study reveals that the title compound crystallizes in a monoclinic crystal system with centrosymmetric space group $P2_1/c$ with lattice parameters; a = 17.1467(10), b = 11.0395(7), c = 9.5821(5) Å β= 98.43(2)°. The packing diagram shows that the adjacent molecules are linked through a pair of C-H···O hydrogen bonds forming an inversion dimer. Hirshfeld surface mapped over the properties such as d_{norm}, Electrostatic potential, shape index, curvedness, and energy framework were also analyzed. The in-silico investigation of the title molecule discloses the efficacious for use as a drug in inhibiting breast Cancer.

Keywords: Crystal growth; chalcone; hirshfeld surface analysis; energy frame work; docking; cancer activity.

1. INTRODUCTION

Chalcones are the important constituent of many natural sources and exhibit a variety of biological activities. The, α, β- unsaturated ketones and its analogues are well known for their enormous biological activities and these are attributed to the carbonyl function with the double bond conjugate [1]. This class of compounds is recognized in natural products like fruits, vegetables, spices, etc, due to which chalcone has been a high-profile topic of interest in academic research and industrial uses [2]. These compounds have shown appositeness in clinical chemistry, their origin being from flavonoid makes them display antibacterial [3], anti-inflammatory [4], antifungal [5], anticancer [6], and many others. The combination of cinnamaldehyde in the chalcone with the α,β-unsaturated carbonyl group may increase pharmaceutical efficiency since cinnamaldehyde alone has good biological activity such as antioxidant, anti-leishmanial [7], antimicrobial [8]. The impairment of regulation of Epidermal Growth Factor Receptor mutant ($EGFR^{mut}$) is one common mechanism in cancer progression, overexpression and activation of EGFR has been reported in various types of cancers, such as breast, head, neck, ovarian, and colon [9]. Transforming growth factor alpha (TGF-α) and increased EGFR has been recognized in many cancers , even at an early stage of lung cancer, breast cancer and low- and high-grade gliomas [10]. With the alluring literature survey, we have synthesized a chalcone with a combination of naphthalene ketone and dimethyl-cinnamaldehyde, and efforts were taken to grow it into a single crystal. The structure was verified by single-crystal XRD and the Hirshfeld surfaces analysis was also performed to visualize and quantifies the molecular interactions. As part of our ongoing studies on chalcone derivatives, an attempt was made to synthesize and study one such derivative and communicating the results in this communication.

2. MATERIALS AND METHODS

2.1 Method of Preparation

All chemicals and solvents used were purchased from Sigma Aldrich and Spectrochem as high purity materials and used as such without any further purification.

The reaction was carried out using Claisen-Schmidt condensation reaction by following the procedure [11] and the reaction scheme is shown in Fig. 1 In a 250mL conical flask, 2g (0.01175mol) of 1-(naphthalen-2-yl)ethan-1-one along with 10mL of ethanol was taken and stirred for ten minutes, to which 2.1g(0.01175mol) of (2*E*)-3-[4-(dimethylamino) phenyl]prop-2-enal was added and continued the stirring. After ten minutes, a solution of 10%NaOH (0.3 g, 10 mL) was added and stirred for 2 hours. The resultant mixture was kept overnight at room temperature which was then added with crushed ice to accelerate the dehydration process, leading to a precipitate of the compound, (*2E,4E*)-5-(4-(dimethylamino) phenyl)-1-(naphthalen-2-yl)penta-2,4-dien-1-one (DPNP)(Yield:85%; M.P:119°C, by Melting point apparatus). The product is isolated by filtration and then washed with distilled water several times to remove the trace of NaOH if present in the product. The crude product was then crystallized with a mixture of acetone and EMK (1:2), to give a red block like crystal, of dimension 15 x 3 x 1 mm within a period of 3days, shown in Fig. 2.

2.2 Chemical Characterization-Xrd

The crystal data were collected using a diffraction quality crystal of size 0.40x0.30x 0.25mm on the goniometer head of the BRUKER AXS KAPPA APEX2-CCD diffractometer with MoKα (λ = 0.71073 Å) as an X-ray radiation source from Sophisticated Analytical Instruments Facility(SAIF), IITM, Tamilnadu, Chennai-36. The 3D crystal structure of the title molecule,

$C_{23}H_{21}NO$, was solved and refined using the SHEL-XS 97 [12] and SHEL-XL/XT-14 [13] software, respectively, by employing a full-matrix least-squares procedure on F^2. The Program PLATON a Multipurpose Crystallographic Tool was utilized to calculate the crystal parameters such as bond lengths, bond angles, torsion angles, dihedral angles, intra and intermolecular interactions, and conformation of the ring systems.

2.3 Molecular Interactions-Crystal Explorer 17.5 Software

Hirshfeld surface is described by the molecule and the propinquity of its nearest neighbors encrypted information about intermolecular interactions. Analysis of Hirshfeld surfaces, 2D fingerprint plots, molecular interactions, and the energy framework have been performed using Crystal Explorer 17.5 [14] software program based on the crystallographic information obtained from the XRD technique. The possible interactions in the molecule are studied using the Hirshfeld surface mapped over the properties like d_{norm},shape index, curvedness, and electrostatic potential, and the fragments around the molecule are completed to see the interaction with the neighbouring molecule. Fingerprint plot was generated with d_i(x-axis) and d_e(y-axis) showing the closest internal and external distance from a given point on the Hirshfeld surface. The molecule is selected forming a cluster of radius 3.8Å around the molecule, by completing the fragments around it, to calculate interaction energies at B3LYP/6-31G (p,d) level. The energy framework calculations were performed for cluster molecules present in 2 x 2 x 2unit cells using the CE-B3LYP energy model.

2.4 Molecular Docking [In-Silico] Study-Auto Dock 4.26 Software

The ligand-target interactions were studied using Auto Dock 4.26 software package [15] and PYMOL [16] graphic software was used for the preparation of ligand and target, and viewing the interaction between them. Molecular docking helps us in giving a vision with the search algorithm for the best orientation of small molecules which perfectly fits into the target cavity, which can be used in drug designing and therapy. This is also used to understand the binding orientation and affinity of the molecule and target. Auto dock 4.26 software was used to predict the binding with a receptor in 3D. Crystal Structure of PDB ID: 1M17 [17] was downloaded from RCSB Protein Data Bank [18]. All the water, non-interacting ions, and co-crystal inhibitor were removed. The computation of the atomic charges was done by Kollman and Gasteiger method after the polar hydrogen was attached. The title compound was selected as ligand and a comparative study was done with standard drug erlotinib, which is been used for treating breast cancer, which was downloaded from RCSB data bank [18]. The ligand was converted to PDB format from CIF format using Open Bable software [19]. The active site of the protein was defined with 74 x 60 x 62 Å grid size along x, y, and z-axis and grid spacing 0.375Å with the Lamarckian Genetic Algorithm (LGA) being used to carry out the process [20].

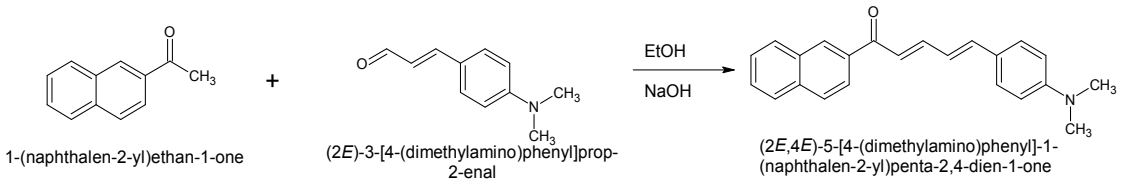

Fig. 1. Reaction scheme of DPNP

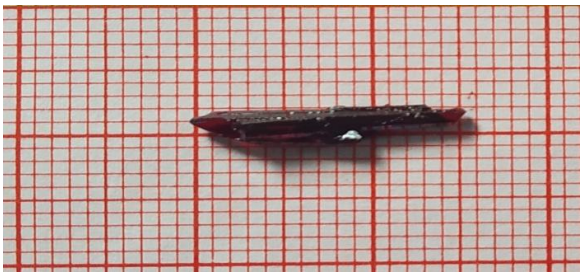

Fig. 2. DPNP crystal

3. RESULTS AND DISCUSSION

3.1 Geometrical Parameters

The crystal data collection and refinement details are tabulated in Table 1. The selected bond lengths and bond angles, and torsion angles are listed in Table 2 and Table 3, respectively. Whereas the hydrogen bond geometry is given in Table 4. The ORTEP plot representing the molecular structure drawn at 30% probability level [21], is shown in Fig. 3. The packing of the molecules within the unit cell viewed along 'b' axis is shown in Fig. 4. The C-C, C-N and C=O bond distances in the structure are lies between 1.309(1)-1.478(1) Å, 1.362(1)-1.443(1)Å, and 1.220(1)Å, respectively, and are comparable with the values of the similar reported structure [11,22]. The C-C-C bond angles (≈ 120°) show that the rings are planar. The sum of the angles around the N atom is 358.14(1)° indicating the sp^2 hybridization of the atom. The torsion angle C11-C12-C13-C14 is 179.8(1)° shows that the α, β unsaturated carbonyl group has an anti-periplanar orientation with the phenyl ring, and this may be due to the di-methylamino group substituent in the molecule [23]. The dihedral angle between the two phenyl rings is 24.68 (1)°, which shows the axial orientation with each other. In the crystal structure, the adjacent molecules are linked through a pair of C-H·O hydrogen bonds (Table 4, Fig. 4) forming inversion dimer described by a graph set motif $R_2^2(26)$ [24]. The C atoms of the naphthalene ring are observed over two sets of sites with refined occupancies of 0.573(7) and 0.427(7).

3.2 Hirshfeld Surfaces Analysis and Energy Framework Investigation

The distribution of weak intermolecular interactions and short contacts in the structure can be visualized and the mapping of the Hirshfeld surface over d_{norm}, (Fig. 5a), curvedness, shape index, and fragment patches have been analyzed for the closeness of the neighbouring molecule. The red spots over the surface indicate the position of close contacts. The possible interactions between the two adjacent molecules involving C-H…O hydrogen bond with D…A (Donor-Acceptor) distance equal to 3.490 Å, is shown in Fig. 5 b.

Table 1. Data collection and refinement details

Crystal data	DPNP
CCDC No.	1985059
Empirical formula	C_{23} H_{21} N O
Formula weight	327.41
Temperature	299(2) K
Wavelength	0.71073 Å
Crystal system	Monoclinic
Space group	P 21/c
Unit cell dimensions	a = 17.1467(10) Å b = 11.0395(7) Å β= 98.430(2)°. c = 9.5821(5) Å
Volume	1794.21(18) Å3
Z	4
Density (calculated)	1.212 Mg/m3
Absorption coefficient	0.074 mm-1
F(000)	696
Crystal size	0.40 x 0.30 x 0.25 mm
Theta range for data collection	3.505 to 24.997°.
Index ranges	-20<=h<=20, -13<=k<=13, -10<=l<=11
Reflections collected	33009
Independent reflections	3144 [R(int) = 0.0431]
Completeness to theta = 24.997°	99.30%
Refinement method	Full-matrix least-squares on F^2
Data / restraints / parameters	3144 / 16 / 265
Goodness-of-fit on F^2	1.17
Final R indices [I>2sigma(I)]	R1 = 0.0785, wR2 = 0.1878
R indices (all data)	R1 = 0.0874, wR2 = 0.1941
Extinction coefficient	n/a
Largest diff. peak and hole	0.215 and -0.174 e.$Å^{-3}$

Table 2. Selected bond lengths [Å] and bond angles [°]

ATOMS	BOND LENGTH [Å]	ATOMS	BOND ANGLE [°]	ATOM	BOND ANGLE [°]
C1A-C2	1.423(1)	C2-C1A-C6	114.1(1)	C14-C15-C16	128.9(1)
C1A-C6	1.450(1)	C4A-C3A-C2	129.7(1)	C21-C16-C17	116.0(1)
C3A-C4A	1.364(1)	C3A-C4A-C5A	114.4(1)	C21-C16-C15	120.8(1)
C3A-C2	1.378(1)	C10A-C5A-C4A	124.2(1)	C17-C16-C15	123.2(1)
C4A-C5A	1.414(1)	C10A-C5A-C6	117.7(1)	C18-C17-C16	121.9(1)
C5A-C10A	1.407(1)	C4A-C5A-C6	118.1(1)	C17-C18-C19	121.4(1)
C5A-C6	1.478(1)	C10A-C9A-C8	121.9(1)	N1-C19-C20	121.8(1)
C9A-C10A	1.338(1)	C9A-C10A-C5A	121.5(1)	N1-C19-C18	121.6(1)
C9A-C8	1.407(1)	C2-C1B-C6	121.9(1)	C20-C19-C18	116.7(1)
C1B-C2	1.350(1)	C4B-C3B-C2	104.4(1)	C21-C20-C19	120.9(1)
C1B-C6	1.407(1)	C3B-C4B-C5B	130.1(2)	C20-C21-C16	123.1(1)
C3B-C4B	1.354(1)	C6-C5B-C10B	118.9(1)	C19-N1-C23	121.3(1)
C3B-C2	1.370(1)	C6-C5B-C4B	117.6(1)	C19-N1-C22	121.3(1)
C4B-C5B	1.424(1)	C10B-C5B-C4B	123.4(1)	C23-N1-C22	116.8(1)
C5B-C6	1.309(1)	C10B-C9B-C8	118.5(1)		
C5B-C10B	1.400(1)	C9B-C10B-C5B	122.1(1)		
C9B-C10B	1.378(2)	C1B-C2-C3B	120.5(1)		
C9B-C8	1.445(1)	C3A-C2-C1A	115.8(1)		
C6-C7	1.403(1)	C5B-C6-C7	120.1(1)		
C7-C8	1.347(1)	C5B-C6-C1B	105.6(1)		
C8-C11	1.486(1)	C7-C6-C1B	126.7(1)		
C11-O1	1.220(1)	C7-C6-C1A	120.8(1)		
C11-C12	1.464(1)	C7-C6-C5A	115.9(1)		
C12-C13	1.343(1)	C1A-C6-C5A	119.1(1)		
C13-C14	1.421(1)	C8-C7-C6	123.4(1)		
C14-C15	1.342(1)	C7-C8-C9A	117.7(1)		
C15-C16	1.443(1)	C7-C8-C9B	115.6(1)		
C16-C21	1.395(1)	C7-C8-C11	119.4(1)		
C16-C17	1.401(1)	C9A-C8-C11	121.2(1)		
C17-C18	1.370(1)	C9B-C8-C11	122.7(1)		
C18-C19	1.411(1)	O1-C11-C12	121.3(1)		
C19-N1	1.362(1)	O1-C11-C8	119.5(1)		
C19-C20	1.403(1)	C12-C11-C8	119.1(1)		
C20-C21	1.365(1)	C13-C12-C11	121.6(1)		
C22-N1	1.443(1)	C12-C13-C14	126.2(1)		
C23-N1	1.442(1)	C15-C14-C13	123.4(1)		

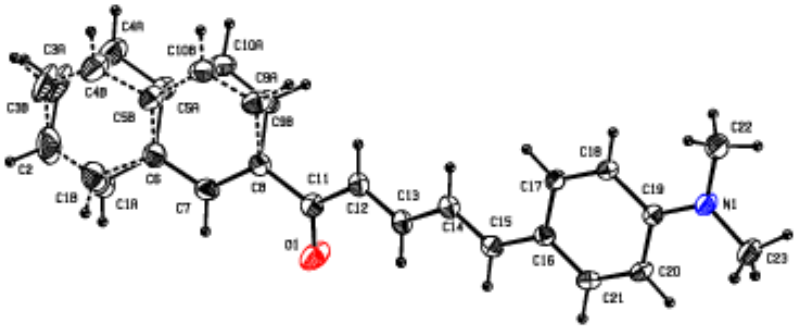

Fig. 3. ORTEP plot with numbering scheme drawn at 30% probability level of the compound

Table 3. Torsional angle [°]

ATOMS	TORSIONAL ANGLE	ATOMS	TORSIONAL ANGLE
C2-C3A-C4A-C5A	-15(1)	C6-C7-C8-C9B	14.6(1)
C3A-C4A-C5A-C10A	-175.1(2)	C6-C7-C8-C11	177.6(1)
C3A-C4A-C5A-C6	5.3(2)	C10A-C9A-C8-C7	9.0(1)
C8-C9A-C10A-C5A	0.9(1)	C10A-C9A-C8-C11	174.1(1)
C4A-C5A-C10A-C9A	177.1(1)	C10B-C9B-C8-C7	-9.8(1)
C6-C5A-C10A-C9A	-3.3(1)	C10B-C9B-C8-C11	-172.2(1)
C2-C3B-C4B-C5B	25(1)	C7-C8-C11-O1	23.3(1)
C3B-C4B-C5B-C6	-16(1)	C9A-C8-C11-O1	-141.5(1)
C3B-C4B-C5B-C10B	168(1)	C9B-C8-C11-O1	-174.9(1)
C8-C9B-C10B-C5B	3.0(2)	C7-C8-C11-C12	-154.4(1)
C6-C5B-C10B-C9B	-0.2(2)	C9A-C8-C11-C12	40.7(1)
C4B-C5B-C10B-C9B	176.2(1)	C9B-C8-C11-C12	7.3(1)
C6-C1B-C2-C3B	-43(1)	O1-C11-C12-C13	-7.4(1)
C4B-C3B-C2-C1B	4(1)	C8-C11-C12-C13	170.3(1)
C4A-C3A-C2-C1A	-2(1)	C11-C12-C13-C14	179.8(1)
C6-C1A-C2-C3A	25.7(2)	C12-C13-C14-C15	-178.3(1)
C10B-C5B-C6-C7	4.3(1)	C13-C14-C15-C16	174.8(1)
C4B-C5B-C6-C7	-172.3(1)	C14-C15-C16-C21	-171.5(1)
C10B-C5B-C6-C1B	155.9(1)	C14-C15-C16-C17	6.4(1)
C4B-C5B-C6-C1B	-20.8(1)	C21-C16-C17-C18	2.0(1)
C2-C1B-C6-C5B	49.5(1)	C15-C16-C17-C18	-176.1(1)
C2-C1B-C6-C7	-161.4(1)	C16-C17-C18-C19	0.5(1)
C2-C1A-C6-C7	169.7(1)	C17-C18-C19-N1	177.2(1)
C2-C1A-C6-C5A	-34.1(1)	C17-C18-C19-C20	-2.4(1)
C10A-C5A-C6-C7	-3.8(1)	N1-C19-C20-C21	-177.8(1)
C4A-C5A-C6-C7	175.8(1)	C18-C19-C20-C21	1.7(1)
C10A-C5A-C6-C1A	-161.2(1)	C19-C20-C21-C16	0.8(1)
C4A-C5A-C6-C1A	18.5(1)	C17-C16-C21-C20	-2.7(1)
C5B-C6-C7-C8	-12.3(1)	C15-C16-C21-C20	175.4(1)
C1B-C6-C7-C8	-157.4(1)	C20-C19-N1-C23	-7.6(1)
C1A-C6-C7-C8	171.3(1)	C18-C19-N1-C23	172.8(1)
C5A-C6-C7-C8	14.4(1)	C20-C19-N1-C22	-178.7(1)
C6-C7-C8-C9A	-17.0(1)	C18-C19-N1-C22	1.7(1)

Table 4. Hydrogen bonds for DPNP [Å ,°]

D-H...A	d(D-H)	d(H...A)	d(D...A)	<(DHA)
C23-H23B...O1#1	0.96	2.48	3.394(4)	159

Symmetry transformations used to generate equivalent atoms: #1 -x+1,-y+1,-z+1

The presence of the π-π stacking interactions can be envisaged with the adjacent red and blue triangles on the Hirshfeld surface mapped over shaped index (Fig. 6a) and as flat regions over the curvedness surface (Fig. 6b). The nearest neighbour coordination of the molecule is 14, found by the number of colour patches (Fig. 6c). The electrostatic potential surface mapped with Hirshfeld surface (Fig. 6d) was obtained using TONTO, integrated in the software program Crystal Explorer 17.5 [25], shows the electronegative atom present in the title compound (red region). The contributions due to the various interactions between the chemical species were analyzed via the 2D fingerprint plots (Fig. 7), where the H…H interactions has the largest contribution to the total Hirshfeld surface of 57.3% with minimum value of de=di≈.2Å, the C…H/H…C contacts offer 31.7% with de+di≈2.4Å, the H-O/O-H contacts supplement 7.3%, followed by the C-C contacts 3.0%,N-H/H-N with 0.5% and C-N/N-C interactions of 0.2%.

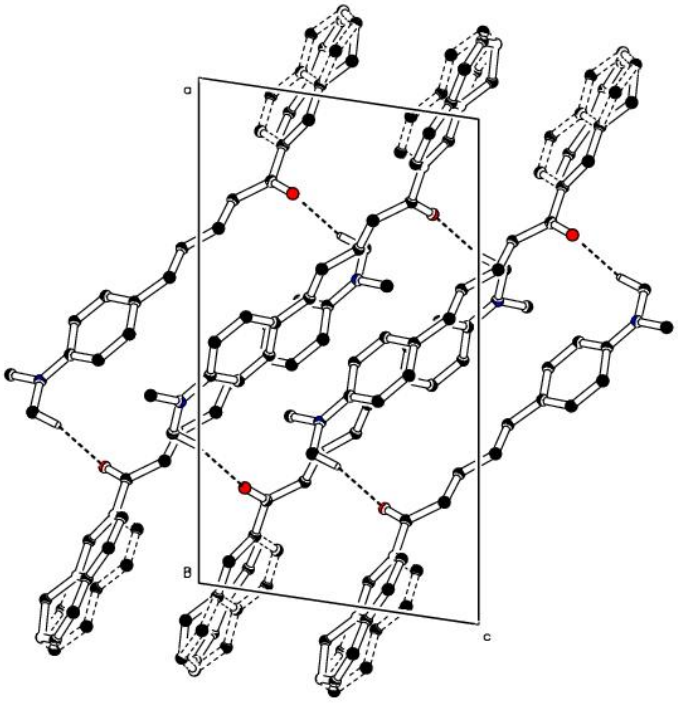

Fig. 4. Packing of the molecules in the unit cell viewed along 'b' axis. The dashed line represents the hydrogen bond

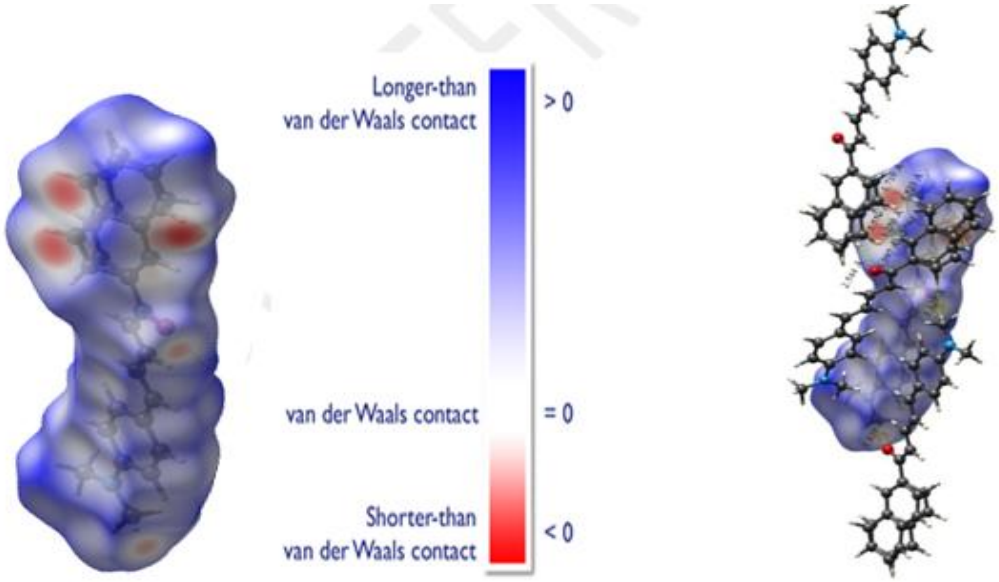

[a] **[b]**

Fig. 5. [a] Hirshfeld surface mapped over d_{norm} and [b] showing the possible intermolecular interactions

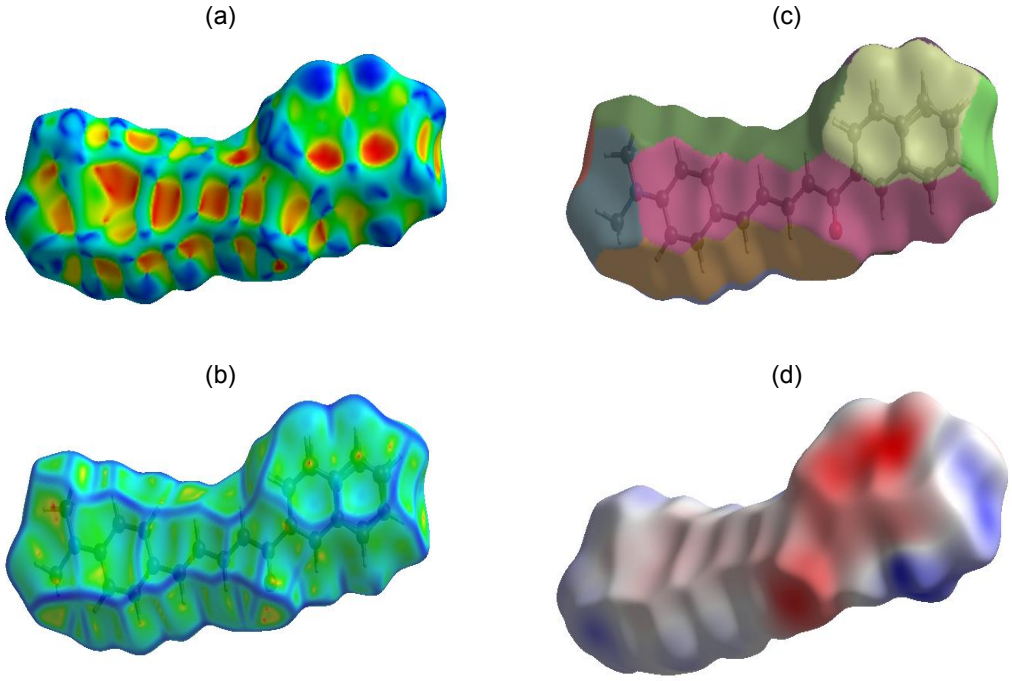

Fig. 6. Hirshfeld surfaces mapped over (a) Shaped Index (b) Curvedness (c) Fragment patches (d) Electrostatic Potentials

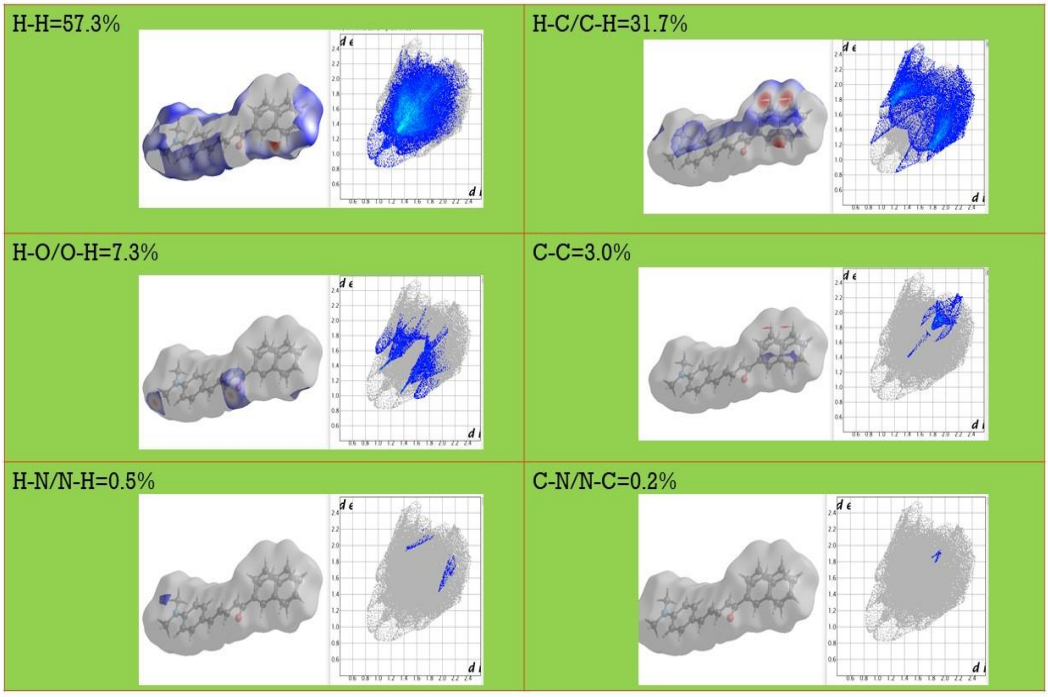

Fig. 7. 2D Fingerprint plots for the title compound showing the contributions of individual types of interactions

With the magnitude of energy framework, we can represent the intermolecular interaction energies using the four components namely, electrostatic, polarization, dispersion, and exchange repulsion. The total energy is the sum of these scaled components, which is generally calculated for a cluster of 3.8 Å radius (Fig. 8a), using CE-B3LYP energy model. The interaction energies calculated for DPNP is shown in Table 5 with the scaling factor used, revealing that the dispersion energy is more significant than other energies. The energies between the molecular pairs are shown as cylinders connecting centroids are shown in Figs. 8b and 8d, electrostatic energy (coulomb) by red cylinders, dispersion energy by green cylinders, and total energy by blue cylinders

3.3 Molecular Docking (In-Silico Analysis)

The active site interactions between the ligand (small molecule) and the target (protein with PDB id: 1M17) is shown in Fig. 9a, while the co-crystal(Erlotinib) binding with protein 1M17 is shown in Fig 9b.To obtain best fit interaction having the lowest binding energy,10 runs were tried using AutoDock Tools 1.5.6, and the value of the scoring function were tabulated in Table 6. The various parameters like binding energy, binding site interactions, and Donor-Acceptor distances were listed in Table 7. The inhibition constant (Ki) for 1M17 with the ligand interaction was found to be 486.54nM, which is the measure of the ligand-binding affinity to protein. The value of Ki is directly proportional to the amount of medication required to inhibit the enzyme's activity [26]. In this work, corresponding to run 2, the ligand interaction with 1M17 protein exhibits a lower binding energy value of -8.61kcal/mol and is comparable with the literature value [27,28]. The lower the binding energy greater will be the molecular stability that directs the interaction between the ligand and the target molecules. The title molecule fits well into the inhibition site of 1M17 protein, with one hydrogen at a distance of 2.731Å. The amino acid residues surrounding the ligand DPNP are similar to that of the co-crystal; Gly 772(A), Leu 694(A), Met 769(A), Ala 719 (A), Thr 766(A), Gln 767(A), Thr 830(A), Met 742(A), Glu 738 (A), Lys 721)A), Asp 831(A), Leu 768(A), Leu 820(A), Pro 770(A), and those are almost with erlotinib used for breast cancer treatment. Lig plot [29] has been plotted for both 1M17 and DPNP and 1M17 with erlotinib interaction, and is shown in Fig. 10a and 10b, respectively.

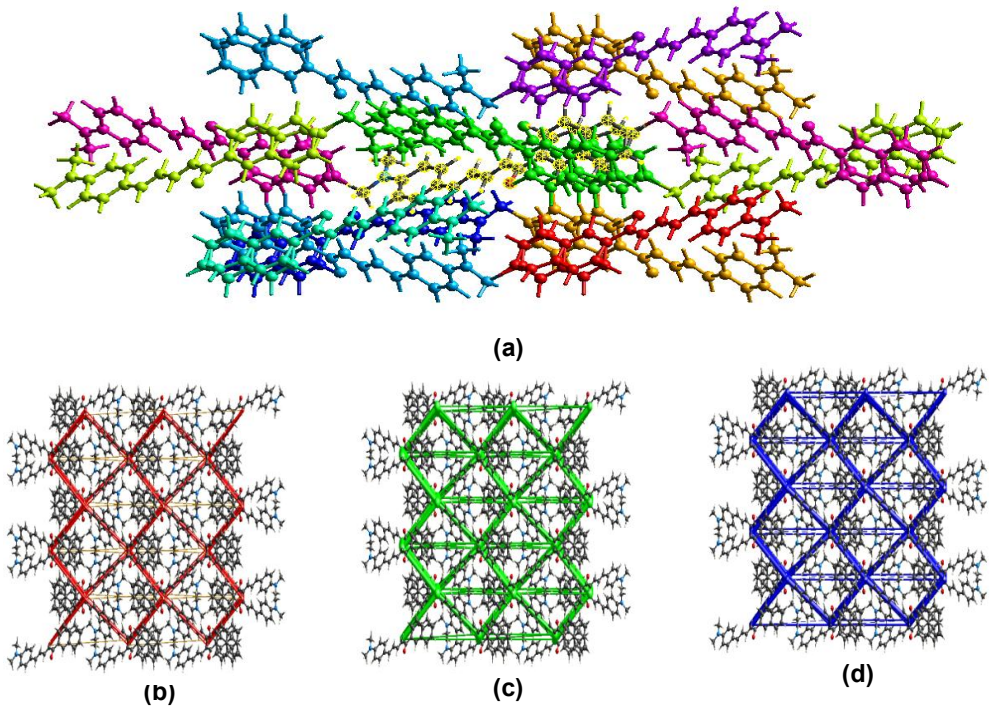

Fig. 8. (a) Interaction between the selected molecule and the molecules present in a 3.8 Å cluster(b) Electrostatic energy (c) Dispersion energy and (d) Total energy

Table 5. Calculated interaction energies for DPNP

N	Smyop	R	Electron Density	E_ele	E_pol	E_dis	E_rep	E_tot
1	-x, -y, -z	10.91	B3LPY/6-31G(d, p)	-22.5	-9.7	-20.8	4.2	-46.4
2	-x, y+1/2, -z+1/2	9.17	B3LPY/6-31G(d, p)	-23.2	-4.5	-54.3	52.7	-42.6
2	x, y, z	18.38	B3LPY/6-31G(d, p)	-2.0	-2.2	-15.4	4.1	-14.7
2	x, -y+1/2, z+1/2	4.83	B3LPY/6-31G(d, p)	-26.0	-11.5	-102.3	126.8	-46.7
1	-x, -y,- z	11.05	B3LPY/6-31G(d, p)	-22.9	-9.5	-34.8	31.3	-42.2
2	-x, y+1/2, -z+1/2	12.44	B3LPY/6-31G(d, p)	-10.7	-2.5	-30.3	25.4	-23.8
1	-x, -y,- z	14.83	B3LPY/6-31G(d, p)	-6.9	-3.8	-52.1	26.4	-39.2
1	-x, -y,- z	11.54	B3LPY/6-31G(d, p)	-31.7	-5.5	-82.1	81.5	-58.7
2	x, -y+1/2, z+1/2	20.71	B3LPY/6-31G(d, p)	5.8	-3.1	-13.8	9.3	-2.4

Energy Model	K_ele	K_pol	K_dis	K_rep
CE-B3LYP/6-31G(d, p)electron densities	1.057	0.740	0.871	0.618

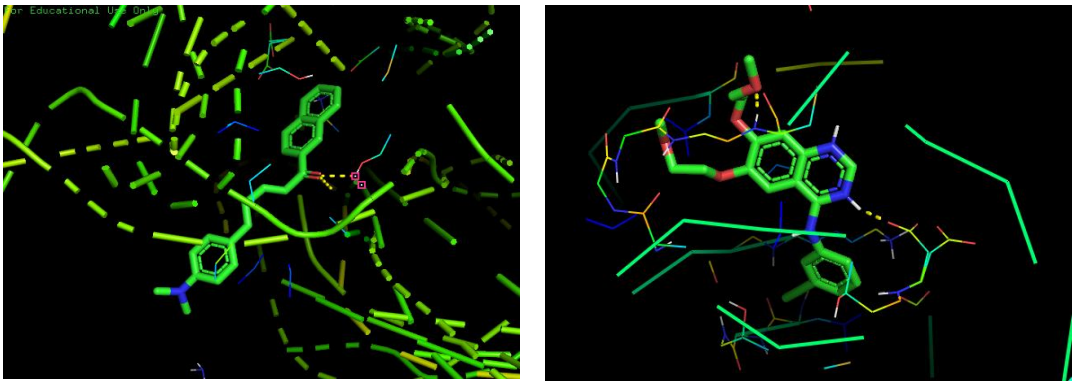

(a) (b)

Fig. 9. PYMOL plot representing the active site interactions (a) Between the ligand (DPNP) and the protein (1M17) (b) Between the co-crystal (erlotinib) and the protein (1M17)

Table 6. Scoring Functions obtained via molecular docking simulation

Run No.	Binding energy kcal/mol	Inhibition constant(Ki)nM	Intermolecular energy kcal/mol
1	-8.34	772.79	-9.83
2	**-8.61**	**486.54**	**-10.10**
3	-8.16	1040.00	-9.65
4	-8.34	776.68	-9.83
5	-8.18	1010.00	-9.67
6	-8.17	1020.00	-9.66
7	-8.37	728.98	-9.86
8	-8.61	491.41	-10.10
9	-8.20	980.51	-9.69
10	-8.18	1000.00	-9.68

Table 7. Binding site interactions and binding energies

Ligand	Run No./Pose	Binding site interaction	D-H…A (Å)	Binding energy kcal/mol
Co-crystal (Erlotinib)	5	N-H...O [Asp 831(A)] [Cys 773(A)]N-H...O	2.70Å 3.11°	-6.70
Title molecule (DPNP)	2	[Thr 766(A)] O-H...O)	2.731Å	-8.61

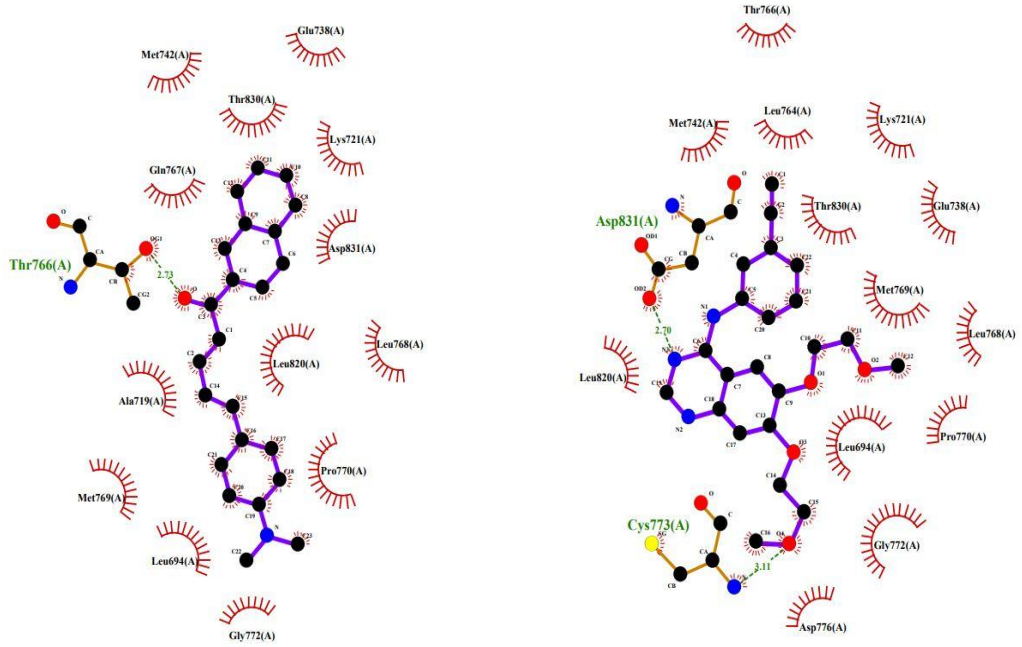

(a) **(b)**

Fig. 10. Lig plot representing the active site interactions (a) Between the ligand (DPNP) and the protein (1M17) (b) Between the co-crystal (erlotinib) and the protein (1M17)

4. CONCLUSION

A new chalcone derivative DPNP has been synthesized by Claisen-Schmidt condensation reaction and by using slow evaporation technique. The as-grown crystal was studied for its 3D structure and crystallographic parameters using the X-ray diffraction technique. The compound was crystallized in monoclinic crystal system with the space group P $2_1/c$, The molecular interactions such as intra and intermolecular hydrogen bonds and the short contacts have been visualized and analyzed via mapping the Hirshfeld surface over d_{norm}, shape index, curvedness using the software Crystal explorer 17.5, and these analysis specifies that the crystal stability is determined by π-π stacking interactions in addition to the hydrogen bonding interactions. The suitability of the title molecule for pharmacological application has been verified by performing in-silico analysis. The observed binding site interactions between the ligand (DNPN) and the target (protein) are comparable with the reference material and clearly demonstrate that the title molecule can be a lead molecule in the field of drug, designing to fight against breast cancer.

ACKNOWLEDGEMENT

The authors thank the Central Instrumentation Facility (DST– FIST), Queen Mary's College (A), Chennai-4 for the computing facility and SAIF, IIT, Madras, for the X-ray data collection facility.

COMPETING INTERESTS

Authors have declared that no competing interests exist.

REFERENCES

1. Singh P, Anand A, Kumar V. Recent developments in biological activities of chalcones: A mini review. European Journal of Medicinal Chemistry. 2014;85:758-77. Available:https://doi.org/10.1016/j.ejmech.2014.08.033
2. Sahu NK, Balbhadra SS, Choudhary J, V Kohli D. Exploring pharmacological significance of chalcone scaffold: A review. Current medicinal chemistry. 2012;19(2):209-25. Available:https://doi.org/10.2174/092986712803414132

3. Ansari FL, Nazir S, Noureen H, Mirza B. Combinatorial synthesis and antibacterial evaluation of an indexed chalcone library. Chemistry & biodiversity. 2005;2(12): 1656-64.
Available:https://doi.org/10.1002/cbdv.200590135
4. Hsieh HK, Tsao LT, Wang JP, Lin CN. Synthesis and anti-inflammatory effect of chalcones. Journal of pharmacy and pharmacology. 2000;52(2):163-71.
Available:https://doi.org/10.1211/0022357001773814
5. Lahtchev KL, Batovska DI, St PP, Ubiyvovk VM, Sibirny AA. Antifungal activity of chalcones: A mechanistic study using various yeast strains. European Journal of Medicinal Chemistry. 2008;43 (10):2220-8.
Available:https://doi.org/10.1016/j.ejmech.2007.12.027
6. Mahapatra DK, Bharti SK, Asati V. Anti-cancer chalcones: Structural and molecular target perspectives. European Journal of Medicinal Chemistry. 2015 ;98:69-114.
Available:https://doi.org/10.1016/j.ejmech.2015.05.004
7. Sharma UK, Sharma AK, Gupta A, Kumar R, Pandey AK, Pandey AK. Pharmacological activities of cinnamaldehyde and eugenol: Antioxidant, cytotoxic and anti-leishmanial aspects. Cell Mol Biol (Noisy le Grand). 2017;63(6).
Available:http://dx.doi.org/10.14715/cmb/2017.63.
8. Montazerozohori M, Mohammadi H, Masoudiasl A, Nasr-Esfahani M, Naghiha R, Assoud A. Crystal structure, DFT study, antimicrobial properties and DNA cleavage potential and thermal behavior of some new mercury complexes. Journal of the Iranian Chemical Society. 2017;14(2): 297-312.
Available:https://doi.org/10.1007/s13738-016-0978-8
9. Ciardiello F, Tortora G. Epidermal growth factor receptor (EGFR) as a target in cancer therapy: Understanding the role of receptor expression and other molecular determinants that could influence the response to anti-EGFR drugs. European Journal of Cancer. 2003;39(10):1348-54.
Available:https://doi.org/10.1016/S0959-8049(03)00235-1
10. Chen GJ, Karajannis MA, Newcomb EW, Zagzag D. Overexpression and activation of epidermal growth factor receptor in hemangioblastomas. Journal of Neuro-oncology. 2010;99(2):195-200.
Available:https://dx.doi.org/10.1007%2Fs11060-010-0125-9
11. Biruntha K, Reuben Jonathan D, MohamoodaSumaya U, DravidaThendral ER, Usha G. (3E)-3-{(2E)-3-[4-(Dimethylamino) phenyl] prop-2-enylidene}-3, 4-dihydro-2H-chromen-4-one. IUCrData. 2018;3(9):x181273.
Available:https://doi.org/10.1107/S2414314618012737
12. Sheldrick GM, SHELXS97 S. University of Göttingen.
13. (a) Sheldrick GM. Crystal structure refinement with SHELXL. Acta Crystallographica Section C: Structural Chemistry. 2015;71 (1):3-8.
Available;https://doi.org/10.1107/S2053229614024218
(b) Sheldrick GM. SHELXT–Integrated space-group and crystal-structure determination. Acta Crystallographica Section A: Foundations and Advances. 2015;71(1):3-8.
Available:https://doi.org/10.1107/S2053273314026370
14. Turner MJ, MacKinnon JJ, Wolff SK, Grimwood DJ, Spackman PR, Jayatilaka D, Spackma MA. Crystal Explorer Ver. 17.5. University of Western Avustralia, Pert; 2017.
15. Morris GM, Goodsell DS, Halliday RS, Huey R, Hart WE, Belew RK, Olson AJ. Automated docking using a Lamarckian genetic algorithm and an empirical binding free energy function. Journal Of Computational Chemistry. 1998;19(14): 1639-62.
Available:https://doi.org/10.1002/(SICI)1096-987X(19981115)19:14%3C1639::AID-JCC10%3E3.0.CO;2-B
16. The PyMOL Molecular Graphics System, LLC, Schrodinger, Version 1 5.0.4; 2009.
17. Stamos J, Sliwkowski MX, Eigenbrot C. Structure of the epidermal growth factor receptor kinase domain alone and in complex with a 4-anilinoquinazoline inhibitor. Journal of Biological Chemistry. 2002;277(48):46265-72.
DOI: 10.1074/jbc.M207135200
18. Available:www.rscb.org
19. O'Boyle NM, Banck M, James CA, Morley C, Vandermeersch T, Hutchison GR. Open Babel: An open chemical toolbox. Journal

of Cheminformatics. 2011;3(1):33. Available:https://doi.org/10.1186/1758-2946-3-33

20. Morris GM, Goodsell DS, Halliday RS, Huey R, Hart WE, Belew RK, Olson AJ. Automated docking using a Lamarckian genetic algorithm and an empirical binding free energy function. Journal of Computational Chemistry. 1998;19(14): 1639-62. Available:https://doi.org/10.1002/(SICI)1096-987X(19981115)19:14%3C1639::AID-JCC10%3E3.0.CO;2-B
21. Farrugia LJ. ORTEP-3 for Windows-a version of ORTEP-III with a Graphical User Interface (GUI). Journal of Applied Crystallography. 1997;30(5):565. Available;https://doi.org/10.1107/S0021889897003117
22. Adam F, Samshuddin S, Ameram N, Samartha L. Crystal structure of 5-[4-(dimethylamino) phenyl]-3-(4-methylphenyl)-4, 5-dihydro-1H-pyrazole-1-carbaldehyde. Acta Crystallographica Section E: Crystallographic Communications. 2015;71(12):10312. Available:https://doi.org/10.1107/S2056989015023294
23. Turov AV, Bondarenko SP, Tkachuk AA, Khilya VP. Effect of Lanthanide Shift Reagents on the Conformation of 2′-Methoxychalcones in Solution. Journal of Structural Chemistry. 2001;42(2):309-11. Available:https://doi.org/10.1023/A:1010523603932
24. Etter MC, MacDonald JC, Bernstein J. Graph-set analysis of hydrogen-bond patterns in organic crystals. Acta Crystallographica Section B: Structural Science. 1990;46(2):256-62. Available:https://doi.org/10.1107/S0108768189012929
25. (a) Spackman MA, McKinnon JJ, Jayatilaka D. Electrostatic potentials mapped on Hirshfeld surfaces provide direct insight into intermolecular interactions in crystals. CrystEngComm. 2008;10(4):377-88. Available;https://doi.org/10.1039/B715227B

    (b) Jayatilaka D, Grimwood DJ, Lee A, Lemay A, Russel AJ, Taylor C, Wolff SK, Cassam-Chenai P, Whitton A. TONTO-a system for computational chemistry; 2005.
26. Sevvanthi S, Muthu S, Raja M. Molecular docking, vibrational spectroscopy studies of (RS)-2-(tert-butylamino)-1-(3-chlorophenyl) propan-1-one: A potential adrenaline uptake inhibitor. Journal of Molecular Structure. 2018;1173:251-60. Available;https://doi.org/10.1016/j.molstruc.2018.07.001
27. Clara TH, Muthu S, Prasana JC. Quantum mechanical, spectroscopic and docking studies of (2E)-1-(4-aminophenyl)-3-(4-benzyloxyphenyl)-prop-2-en-1-one Chalcone derivative by density functional theory–A prospective respiratory drug. Materials Today: Proceedings; 2020. Available;https://doi.org/10.1016/j.matpr.2020.08.804
28. Yousuf Z, Iman K, Iftikhar N, Mirza MU. Structure-based virtual screening and molecular docking for the identification of potential multi-targeted inhibitors against breast cancer. Breast Cancer: Targets and Therapy. 2017;9:447. Available:https://dx.doi.org/10.2147%2FBCTT.S132074
29. Laskowski RA, Swindells MB. LigPlot+: multiple ligand–protein interaction diagrams for drug discovery. Available:https://doi.org/10.1021/ci200227u

Peer-review history:
The peer review history for this paper can be accessed here:
http://www.sdiarticle4.com/review-history/64778